Available online at www.sciencedirect.com

SciVerse ScienceDirect

Ceramics International 39 (2013) 2239–2246

CERAMICS INTERNATIONAL

www.elsevier.com/locate/ceramint

Mn_2O_3/TiO_2 nanofibers with broad-spectrum antibiotics effect and photocatalytic activity for preliminary stage of water desalination

Gopal Panthi[a,1], Ayman Yousef[a,b,1], Nasser A.M. Barakat[c,d,*], Khalil Abdelrazek Khalil[e], Shahina Akhter[f], Yu Ri Choi[d], Hak Yong Kim[d,**]

[a]*Bionano Systems Engineering Department, Chonbuk National University, Jeonju 561-756, Republic of Korea*
[b]*Faculty of Engineering, Matteria, Helwan University, Cairo, Egypt*
[c]*Chemical Engineering Department, Faculty of Engineering, Minia University, El-Minia, Egypt*
[d]*Department of Organic Materials and Fiber Engineering, Chonbuk National University, Jeonju 561-756, Republic of Korea*
[e]*Mechanical Engineering Department (NPST), King Saud University, P.O. Box 800, Riyadh 11421, Saudi Arabia*
[f]*Department of Microbiology and Genetics and Institute for Medical Science, Chonbuk National University, Jeonju 561-712, South Korea*

Received 3 August 2012; received in revised form 22 August 2012; accepted 23 August 2012
Available online 10 September 2012

Abstract

Composite nanofibers consisting of Mn_2O_3 and TiO_2 were prepared by the electrospinning process, and tested as Gram-class-independent antibacterial agent and photocatalyst for organic pollutants degradation. Initially, electrospinning of a sol–gel consisting of titanium isopropoxide, manganese acetate tetrahydrate and poly(vinyl pyrrolidone) was used to produce hybrid polymeric nanofibers. Calcination of the obtained nanofibers in air at 650 °C led to produce good morphology Mn_2O_3/TiO_2 nanofibers. Scanning electron microscopy (SEM) and transmission electron microscopy (TEM) were employed to characterize the as-spun nanofibers and the calcined product. X-ray powder diffractometry (XRD) analysis was also used to characterize the chemical composition and the crystallographic structure of the sintered nanofibers. The antibacterial activity of Mn_2O_3/TiO_2 nanofibers against Gram negative and Gram positive bacteria was investigated by calculating the minimum inhibitory concentration after treatment with the nanofibers. Investigations revealed that the lowest concentration of Mn_2O_3/TiO_2 nanofibers solution inhibiting the growth of *Staphylococcus aureus* ATCC 29231 and *Escherichia coli* ATCC 52922 strains is 0.4 and 0.8 μg/ml, respectively. Incorporation of Mn_2O_3 significantly improved the photodegradation of methylene blue (MB) dye under the visible light irradiation due to enhancing rutile phase formation in the TiO_2 nanofibers matrix.

Keywords: Mn_2O_3/TiO_2 nanofibers; Electrospinning; Photocatalytic activity; Broad-spectrum antibiotics

1. Introduction

Over the past decades, considerable attention with respect to environmental problems has been devoted to the development of photocatalytic systems [1–3]. Photocatalysts [4–6] have attracted a great deal of interest due to photoelectrochemical solar-energy conversion. The photocatalysts could be applied for the potential field including water splitting, self-cleaning surfaces, anti-microbial systems, and the decomposition of organic pollutants [7–10].

Electrospinning is a novel and efficient fabrication process that can be utilized to assemble fibrous polymer mats composed of fiber diameters ranging from several microns down to fibers with diameter lower than 100 nm. This electrostatic processing method uses a high-voltage electric field to form solid fibers from a polymeric fluid stream (solution or melted) delivered through a millimeter-scale nozzle. When the diameters of polymer fiber materials are shrunk from micrometers to submicrons or nanometers, there appear several amazing characteristics such as very large surface area to volume ratio (this ratio for a nanofiber

*Corresponding author at: Department of Organic Materials and Fiber Engineering, Chonbuk National University, Jeonju 561-756, Republic of Korea. Tel.: +82 63 270 2363; fax: +82 63 270 2348.
**Corresponding author.
E-mail addresses: nasser@jbnu.ac.kr (N.A.M Barakat), khy@jbnu.ac.kr (H.Y. Kim).
[1]These authors have the same contribution.

0272-8842/$ - see front matter © 2012 Elsevier Ltd and Techna Group S.r.l. All rights reserved.
http://dx.doi.org/10.1016/j.ceramint.2012.08.068

can be as large as 103 times of that of a microfiber), flexibility in surface functionalities, and superior mechanical performance (e.g. stiffness and tensile strength) compared with any other known form of the material. These outstanding properties make the polymer nanofibers to be optimal candidates for many important applications.

Several important semiconductor metal oxides such as TiO_2 [11], ZnO [12], NiO [13], ZnS [14], and Bi_2O_3 [15] nanofibers were fabricated by electrospinning. They not only show photocatalytic efficiency toward the degradation of methylene blue, Rhodamine B and phenol, but also have good reclaiming ability. In order to enhance the photocatalytic activity of single component nanofibers, composite nanofibers with two components such as ZnO/TiO_2 [16], SnO_2/TiO_2 [17], TiO_2/CdO [18], and CuO/TiO_2 [19] composite nanofibers were also prepared.

Manganese oxide materials have lot of applications including catalysis, ion exchange, molecular adsorption, electrode materials for lithium cathodes [20–24] and antibacterial agent [25] due to their structural flexibility combined with novel chemical and physical properties. Although manganese oxide occurs in various oxidation states, MnO, Mn_2O_3, and Mn_3O_4 are the most common form. Polymorphs of Mn_2O_3 have been employed as environmental friendly catalysts to remove carbon monoxide and nitrogen oxide from waste gases [26]. Mn_2O_3 has been synthesized by various methods. Gui et al. [27] synthesized Mn_2O_3 nanocrystals (9–12 nm in diameter) by direct reduction of aqueous $KMnO_4$ with hydrazine solution at ambient temperature. γ-Mn_2O_3 nanowires were synthesized by treatment of α-MnO_2 with ethanol at 140 °C [28]. He et al. [29] prepared nanocrystals of γ-Mn_2O_3 (50 nm) by autoclaving β-MnO_2 with ethanol at 130 °C for 24 h under autogenous pressure.

Recently, TiO_2 nanofibers have attracted a lot of attention due to the huge potential for a wide range of applications. Although several TiO_2 nanocomposites with antimicrobial capabilities have been reported, there are still barriers in their antibacterial application under dark conditions. It has been known that pure TiO_2 exhibits low photocatalytic property due to rapid recombination of the photoactivated electrons and holes. Doping with metal or metal oxide shows an improvement of photocatalytic activity and disinfection effect. As previously reported, doping TiO_2 with metal oxides ZnO [17], CuO [20], SnO_2 [30] or metallic ions Fe^{3+} [31], and Ag [32] enhances the photocatalytic activity and antibacterial activity.

The objective of this research was to synthesize the Mn_2O_3/TiO_2 nanofibers using precursor manganese acetate tetrahydrate and titanium isopropoxide by the electrospinning technique. The photocatalytic activity of thus prepared Mn_2O_3/TiO_2 nanofibers was examined toward methylene blue as a common model for the organic pollutants. Antimicrobial activity against *E. coli* ATCC 52922 (*E. coli*) and *S. aureus* ATCC 29231 (*S. aureus*) was assessed in vitro, and an attempt was made to find the minimum inhibitory concentration of the nanofibers capable of inhibiting the growth of the above mentioned pathogenic strains. To the best of our knowledge, for the first time, we offer supportive evidences to indicate that Mn_2O_3/TiO_2 nanofibers can inhibit bacterial growth and even kill the cells by destroying bacterial membranous structure.

2. Experimental

2.1. Materials

Titanium isopropoxide (TIIP), poly(vinyl pyrrolidone) (PVP) and manganese acetate tetrahydrate (MnAc) were purchased from Aldrich. Analytical grade ethanol was used as solvent. All the materials were used without any further purification.

2.2. Fabrication of TiO_2 nanofibers and Mn_2O_3/TiO_2 nanofibers

Titania nanofibers and Mn_2O_3/TiO_2 nanofibers were prepared by a sol–gel process as reported [20]. Typically, to prepare pristine TiO_2 nanofibers, 1 g TIIP was added to a solution consisting of 2 g acetic acid and 2 g ethanol, the mixture was stirred for 15 min, then 6 g ethanol and 1 g PVP were added to prepare the mixture, stirring was continued until getting yellow transparent sol–gel. The prepared sol–gel was subjected to the electrospinning process. A copper pin (anode) was inserted into the sol–gel solution which was placed in a plastic syringe, and the negative electrode (cathode) was connected with a rotating steel drum (collector) covered by polyethylene sheet. The colloidal solution was briefly electrospun at 20 kV and a 15 cm working distance (the distance between the needle tip and the collector). It is noteworthy mentioning that a simple electrospinning setup was used, no syringe pump was utilized, the syringe was just placed horizontally to prevent the sol–gel from dropping down. The formed nanofiber mats were initially dried for 24 h at 60 °C under vacuum and then calcined in air at 650 °C for 1 h, with a heating rate of 5 °C/min. To synthesize Mn_2O_3/TiO_2 nanofibers, 50 mg MnAc was added to the TIIP/PVP sol–gel prepared by the same aforementioned procedure. After good stirring process, the obtained colloid was subjected to electrospinning and calcination processes using the same previously explained conditions.

2.3. Antibacterial activity of the Mn_2O_3/TiO_2 nanofibers

The bactericidal activity of the Mn_2O_3/TiO_2 nanofibers produced was tested using growth inhibition studies against Gram-positive and Gram-negative bacteria. The pathogens tested in the present study were *S. aureus* ATCC 29231 and *E. coli* ATCC 52922 purchased from the American Type Culture Collection (ATCC). The inoculums were prepared from fresh overnight broth cultures (Trypton soy broth with 0.6% yeast extract—Torlak, Belgrade; final pH 7.3) that were incubated at 37 °C. For antibacterial assay, the bacterial strains were first grown on solid nutrient agar medium and from the agar plates; fresh colonies were inoculated into

100 ml of nutrient broth medium. Growth was monitored at every 3 h under a UV–visible spectrophotometer (Shimadzu, UV-2550), till the optical density (OD) reached 0.1 at 600 nm of 0.1 corresponded to a concentration of 10^8 CFU/ml of medium. Subsequently, 1 ml from the above was further added to 100 ml of freshly prepared nutrient broth medium supplemented with 0.4, 0.8, 1.6, 3.2, 6.4 μg/ml of Mn_2O_3/TiO_2 nanofibers solution. Control broth solution without nanofibers solution was also used. All the flasks were incubated at 37 °C in a rotary shaker with shaking at 150 rpm. The growth rates and the bacterial concentrations were monitored by measuring the OD at 600 nm by a UV spectrophotometer for 10 h. Similarly, antibacterial activity of the as-prepared nanofibers was tested on *E. coli* by the disk susceptibility test. In this method, 100 μL of diluted bacterial suspension (10^8 CFU/mL) was spread on nutrient agar plate and then incubated at 37°C for 24 h. The diameter of the inhibition zones were measured with transparent ruler.

2.4. Sunlight photocatalytic activity test of Mn_2O_3/TiO_2 nanofibers

The photocatalytic degradation of the methylene blue (MB) was carried out in a simple photoreactor. The reactor was a simple laboratory glass bottle of 70 ml capacity. The photocatalytic degradation was carried out at the same conditions on sunny days between 9 a.m. and 12 p.m. in June. The ambient temperature was 25 °C. 50 ml (10 ppm) MB aqueous solution and 25 mg of the catalyst were added to the bottle and magnetically stirred under the sunlight radiation. At specific time intervals, a 2 ml sample was taken out and centrifuged to separate the residual nanofibers catalyst. The concentration of the dye in the withdrawn samples was investigated using a UV–visible spectrophotometer.

2.5. Characterization

The surface morphology of the as-obtained nanofibers was studied by a JEOL JSM-5900 scanning electron microscope (JEOL Ltd., Japan). The phase and crystallinity of the catalyst were characterized using a Rigaku X-ray diffractometer (Rigaku Co., Japan) with Cu Kα ($\lambda = 1.54056$ Å) radiation over a range of 2θ angles from 10° to 80°. High-resolution images and selected area electron diffraction patterns were observed by a JEOL JEM-2200FS transmission electron microscope (TEM) operating at 200 kV equipped with EDX (JEOL Ltd., Japan).

3. Results and discussion

3.1. Phase morphology

Fig. 1A and B shows the SEM images of the electrospun MnAc/TIIP/PVP nanofibers mats and the corresponding powder after sintering; Fig. 1C and D. As shown in this figure the as-obtained nanofibers are in random orientation due to the bending instability accompanied with the

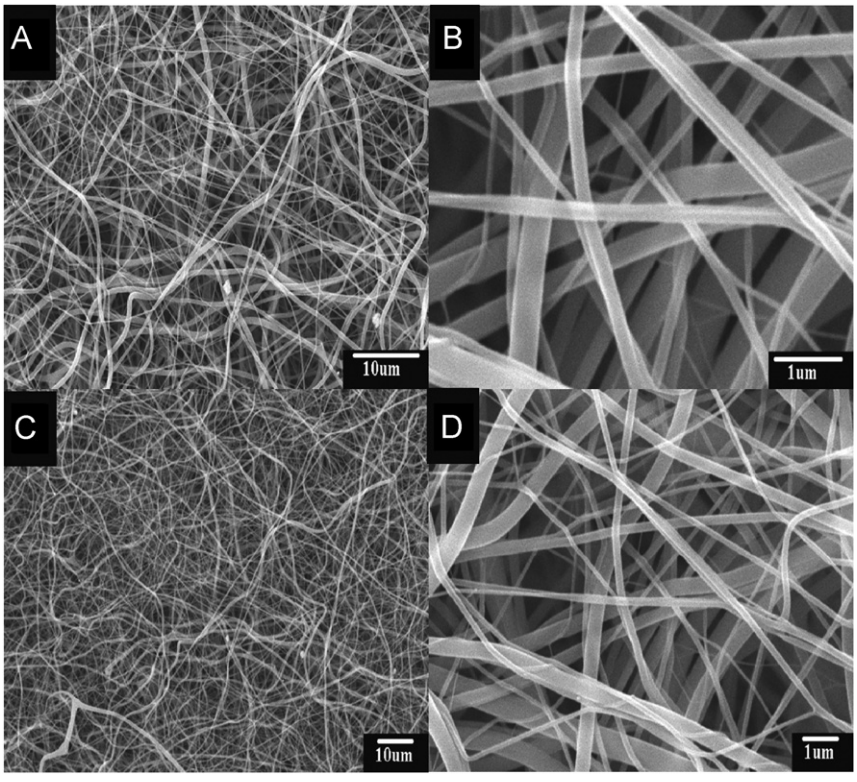

Fig. 1. SEM images of the electrospun MnAc/TIIP/PVP nanofibers mat after drying at 60 °C for 24 h (A, B), and of the produced nanofibers after calcination in air at 650 °C (C, D).

spinning jet. Moreover, it is shown that these random nanofibers had smooth and continuous surfaces. Interestingly, the high calcination temperature did not affect the nanofibrous morphology. In other word, nanofibers keep their structures as good nanofibers after the sintering process.

3.2. Phase structure

To investigate the crystallinity of the obtained nanofibers, XRD analysis was carried out. Fig. 2 demonstrates the XRD patterns of the produced nanofibers. As shown in the figure, calcination of the MnAc-free electrospun nanofibers resulted in producing tetragonal rutile phase TiO_2 nanofibers (JCPDS 21-1276) at 2θ values 27.4°, 36.1°, 39.2°, 41.2°, 44.1°, 54.3°, 56.6°, 62.7°, 64.00°, 69.00°, and 69.8° that corresponding to (110), (101), (200), (111), (210), (211), (220), (002), (310), (301), and (112) crystal planes, respectively. In the same spectra, anatase phase with a tetragonal structure (JCP DS 21-1272) peaks at 2θ values 25.2°, 37.8°, 38.6°, 48°, 62.7°, and 75.00° that correspond to (101), (004), (112), (200), (204), and (215) crystal planes, respectively can be detected. It is noteworthy mentioning that, according to the XRD data, in these pristine TiO_2 nanofibers, anatase and rutile have almost the same content. In the case of the nanofibers obtained from calcination of MnAc-containing electrospun nanofibers, new peaks are observed at 23.66°, 32.24°, 38.02°, 48.0°, 61.00°, and 67.09° that correspond to (211), (222), (400), (431), (611), and (631) crystal planes respectively. These peaks can be assigned to Mn_2O_3 (JCPDS 41-1442). Disappearing of the anatase peaks in the spectra corresponding to the Mn-containing nanofibers is a notable observation. From this new finding, it can be seen that both the incorporation of Mn ions and the calcination process affected the rate of anatase to stable rutile (A–R) phase transformation. Incorporation of Mn ions decreases the onset A–R phase transformation temperature and supports the nucleation and growth of rutile grains. Once formed, rutile grains consume the surrounding anatase matrix and transform them synchronously [33].

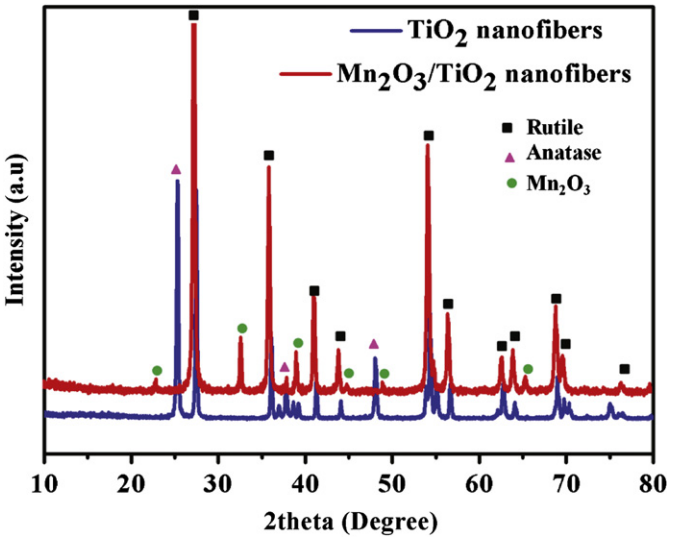

Fig. 2. XRD patterns of the powder obtained after calcination at 650 °C of MnAc/TIIP/PVP and TIIP/PVP in air atmosphere.

According to the crystal lattice parameters, Mn_2O_3 and TiO_2 cannot combine in a single crystal. Accordingly, a main TiO_2 nanofiber doped with Mn_2O_3 nanoparticles is the expected structure of the obtained product. To affirm this, TEM analysis has been conducted. As displayed in Fig. 3A, the tinny black particles distributed along the nanofibers can be observed. The HR TEM image Fig. 3B shows that the black nanoparticles (marked area) have different crystal lattice parameters than the matrix as the crystal plane is closer, so we can claim that these nanoparticles represent Mn_2O_3. The SAED pattern of the marked area (inset of Fig. 3B) shows a different phase structure of the black nanoparticles compared with TiO_2 nanofibers, this affirms the aforementioned conclusion about the doping structure of the introduced Mn_2O_3/TiO_2 nanofibers and simultaneously reveals good crystallinity. In order to understand the composition of the obtained nanofibers, TEM EDX has been carried out; the results are demonstrated in Fig. 4. Fig. 4A represents the normal TEM image, as shown in the figure we can see black color crystalline nanoparticles of Mn_2O_3 along with the nanofibers. Fig. 4B–D represents the line EDX analysis

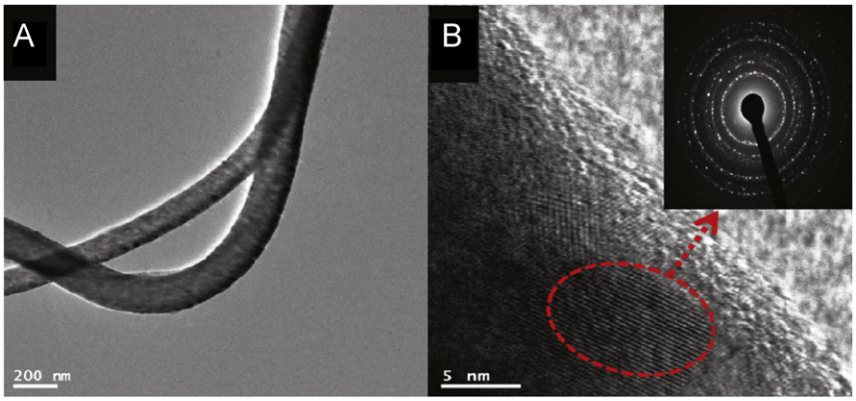

Fig. 3. TEM (A) and HR TEM (B) images for Mn_2O_3/TiO_2 nanofiber. The inset of (B) represents the SAED of the marked area.

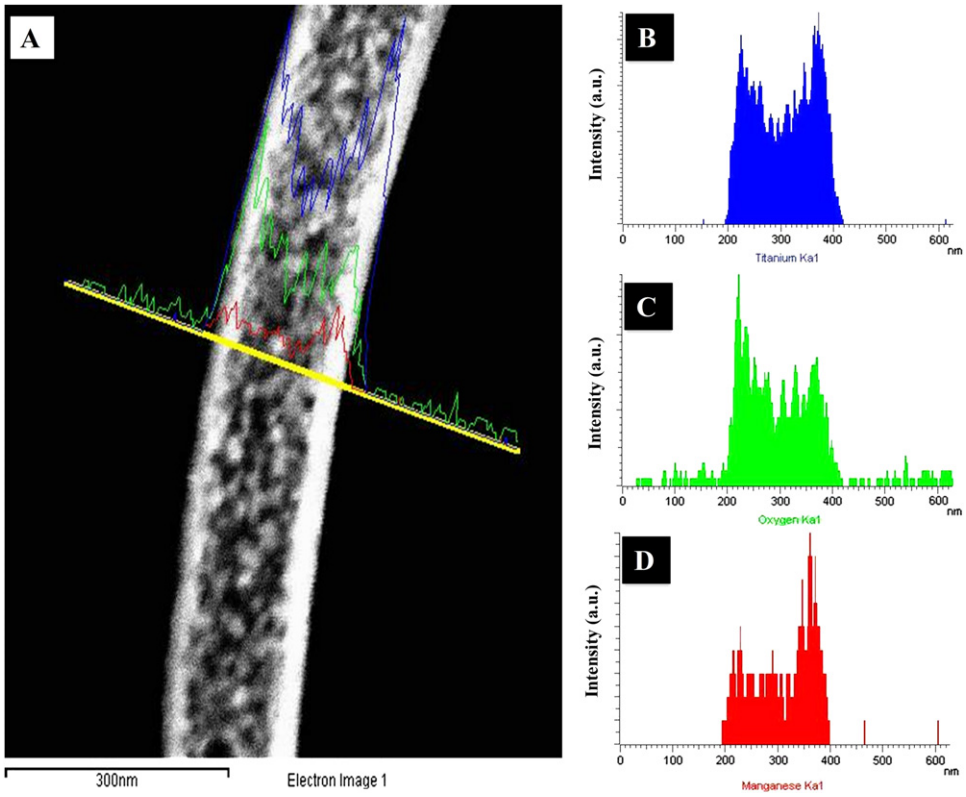

Fig. 4. TEM image for a single Mn_2O_3/TiO_2 nanofiber along with the line TEM EDX analysis: (A) and the corresponding Ti (B), O (C), and Mn (D) line analyses TEM EDX.

of Ti, O, and Mn elements, respectively. This further confirmed the incorporation of Mn_2O_3 nanoparticles in TiO_2 nanofibers. As shown in the figures, Ti and O have almost same distribution, however Mn has distinct peaks, so we can confidently say that Mn_2O_3-doped TiO_2 nanofibers is the structure of the produced powder.

3.3. Antibacterial activity of Mn_2O_3/TiO_2 nanofibers

S. aureus can cause a range of illnesses, from minor skin infections, such as pimples, impetigo, boils (furuncles), cellulitis folliculitis, carbuncles, scalded skin syndrome, and abscesses, to life-threatening diseases such as pneumonia, meningitis, osteomyelitis, endocarditis, toxic shock syndrome (TSS), bacteremia, and sepsis. Its incidence ranges from skin, soft tissue, respiratory, bone, joint, endovascular to wound infections. It is still one of the five most common causes of nosocomial infections and is often the cause of postsurgical wound infections. Each year, some 500,000 patients in American hospitals contract a staphylococcal infection.

E. coli is a Gram-negative, rod-shaped bacterium that is commonly found in the lower intestine of warm-blooded organisms, most *E. coli* strains are harmless. The harmless strains are part of the normal flora of the gut, and can benefit their hosts by producing vitamin K_2, and by preventing the establishment of pathogenic bacteria within the intestine. *E. coli* is the most widely studied prokaryotic model organism and an important species in the fields of biotechnology

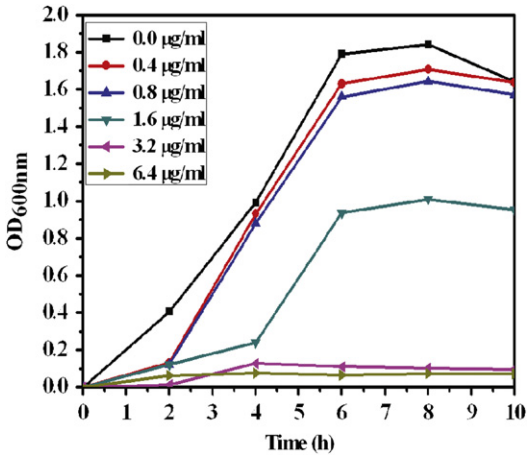

Fig. 5. Growth curve of *E. coli* cells exposed to different concentrations of Mn_2O_3/TiO_2 nanofibers.

and microbiology, where it has served as the host organism for the majority of work with recombinant DNA.

The growth curves of *E. coli* and *S. aureus* treated with nanofibers were shown in Figs. 5 and 6, respectively by measuring optical density at 600 nm in the presence of 0.0, 0.4, 0.8, 1.6, 3.2, and 6.4 μg/ml of Mn_2O_3/TiO_2 nanofibers. The growth curves of the tested strains include three phases: lag phase, exponential phase, and stabilization phase. However, decline phases in each growth curve could not be revealed because we only assayed the total numbers of

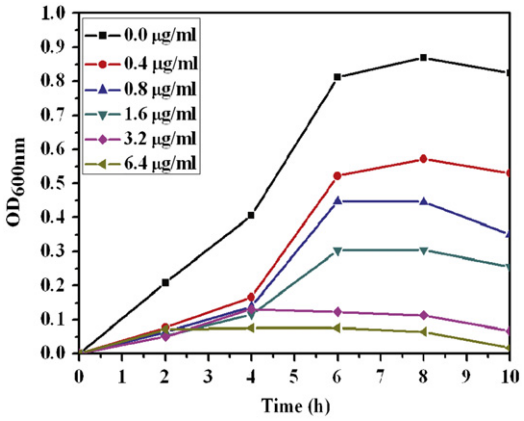

Fig. 6. Growth curve of *S. aureus* cells exposed to different concentrations of Mn_2O_3/TiO_2 nanofibers.

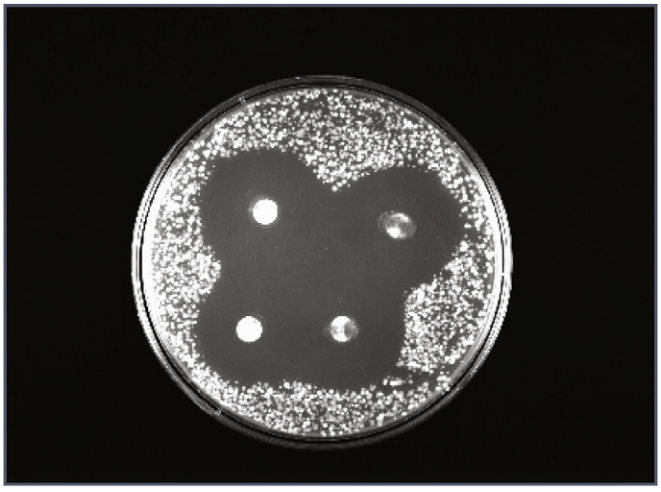

Fig. 7. Inhibition zone test on *E. coli* by Mn_2O_3/TiO_2 nanofibers.

bacteria, including live and dead ones, based on the value of OD 600. Under the absence of Mn_2O_3/TiO_2 nanofibers, both the organisms reached exponential phase rapidly. But exposed to the above mentioned concentrations of nanofibers, *E. coli* cells and *S. aureus* were lagged to 3–4 h, respectively. With the increasing concentration of nanofibers, the delay was more evident. It has been observed that the minimum inhibitory concentration (MIC) defined as the lowest concentration of the Mn_2O_3/TiO_2 nanofibers solution that inhibits growth of the microbial strain is found to be 0.8 and 0.4 μg/ml for *E. coli* and *S. aureus*, respectively. However, in the case of both the microbial strains, it has been seen that with increase in concentration of Mn_2O_3/TiO_2 nanofiber solution, the growth of inhibition has also increased. Noticeable difference in the growth rate has been observed for *E. coli* and *S. aureus* after 4–8 h of incubation with Mn_2O_3/TiO_2 nanofibers solution; the highest concentration (6.4 μg/ml) of the nanofiber solution has been found to exhibit excellent toxicity against both the pathogenic strains tested. Similarly, the effect of Mn_2O_3/TiO_2 nanofibers on *E. coli* was observed by observing the zone of inhibition. As shown in Fig. 7, larger zone of inhibition (around 20 mm) can be seen around the nanofiber disk. Therefore, from this observation we can further claim that Mn_2O_3/TiO_2 nanofibers demonstrate excellent antibacterial properties.

3.4. Photocatalytic activity of Mn_2O_3/TiO_2 nanofibers

Dye degradation is a common strategy to investigate the photocatalytic activity of various compounds. To safely estimate the dye concentration in distilled water, the absorbance intensities of the utilized methylene dye have been measured for many dye/distilled water solutions. The UV absorbance spectra for different concentrations of dye solutions (starting from 1 to 8.75 mg/l) were measured within the range of 500–800 nm Fig. 8A reveals the obtained results. As shown in this figure, the absorbance curves have maximum value at almost 664 nm. Moreover, the maximum measured absorbance intensities were linearly increased with increasing of the dye concentration as shown in Fig. 8B which represents the relationship between the dye concentration and the measured absorbance at

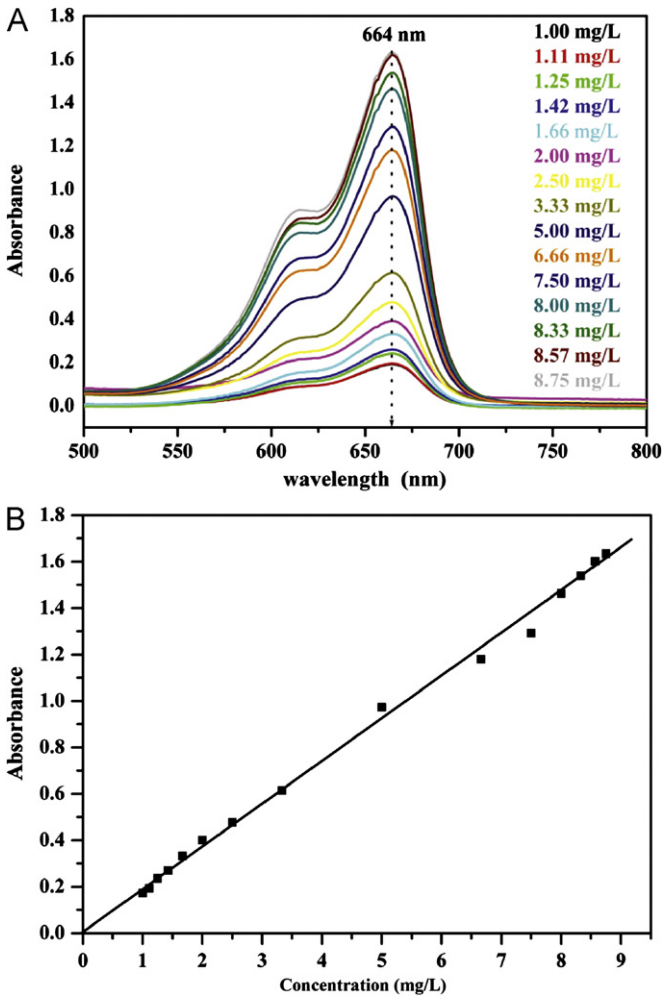

Fig. 8. Absorbance spectra at different concentrations of methylene blue dye solutions within a range of 500–800 nm (A), and the relationship between the absorbance intensity and concentration of the dye at wavelength of 664 nm (B).

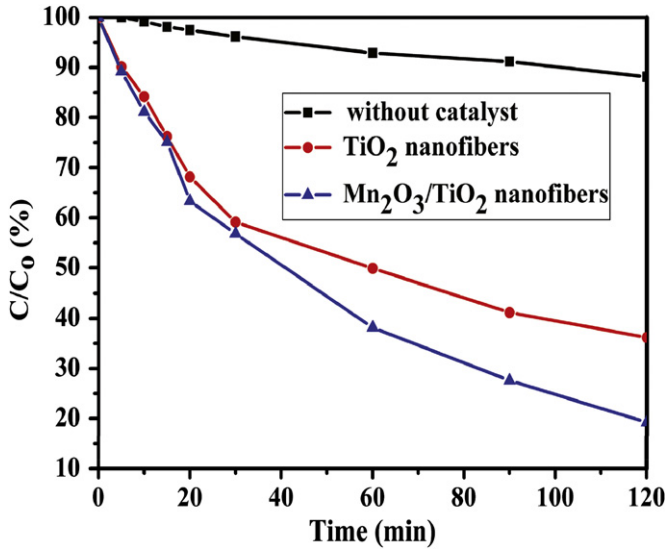

Fig. 9. Degradation profile of the MB dye under sunlight in presence of TiO_2 and Mn_2O_3/TiO_2 nanofibers.

664 nm. As shown in this figure, the absorbance varies linearly with the dye concentration in good linear model. Statistical analyses of this curve indicated high accuracy of the exploited linear model since the coefficient of determination; R^2 of this model was 0.9989 which reveals excellent precision and reproducibility of this calibration curve.

The degradation rate of MB without any catalyst was performed and it could not help more than 10% even after 120 min. Significant increase in the degradation rate of MB dye was found using the Mn_2O_3/TiO_2 nanofibers (Fig. 9). In particular, after 120 min about 90% of the dye was degraded. This result could be due to synergetic coupling effect between (Mn_2O_3 and TiO_2), and due to the high surface area of the nanofibers. However, in the case of pure TiO_2 nanofibers, almost 40% of the dye was oxidized after 120 min. Enhancement of the photocatalytic activity of the composite nanofibers compared to the pristine TiO_2 can be explained by the increase in the rutile content in the composite nanofibers. In the visible light, it is known that rutile has higher photocatalytic activity compared to anatase which is active only under UV light.

3.5. Mechanism of antibacterial and photocatalytic activities of the Mn_2O_3/TiO_2 nanofibers

It can be assumed that the antibacterial activity of Mn_2O_3/TiO_2 nanofibers prepared in our study is mediated by the Mn_2O_3 phase. Gram-positive bacteria have one autoplasic membrane and thick wall composed of multi layers of peptidoglycan, whereas Gram-negative bacteria have a more complex cell wall structure with layer of peptidoglycan between the outer membrane and cytoplasmic membrane. In both cases, antibacterial activity of Mn_2O_3/TiO_2 nanofibers can be attributed to the damage of cell membrane which leads to the leakage of cell content and cell death. The overall charge on the bacterial cell surface at biological pH value is negative due to excess number of carboxylic and other groups that upon dissociation make cell surface negative [34]. Therefore, adhesion of nanofibers with negatively charged bacterial cell membrane takes place by means of Mn^{3+} ions present in nanofibers. Although the exact mechanism for the damage of cell membrane is not clear and it is still under discussion, several researchers have tried to explain the damage of bacterial cell wall is due to the incorporation of foreign materials. But more studies are required to conclude the relation of antibacterial activity with Mn_2O_3/TiO_2 nanofibers.

The higher photocatalytic activity of Mn_2O_3/TiO_2 nanofibers for the degradation of MB dye can be explained due to involvement of Mn^{3+} moieties as Mn_2O_3 in the nanofibers. The presence of such moieties was responsible for improving electronic and thus optical properties of these nanofibers. Initially, unstable dye cation is formed by sensitizing it with catalyst in the presence of visible light and gets decomposed injecting electron to the conduction band of TiO_2 leaving hole in the valence band, which is captured by Mn^{3+} producing Mn^{4+} or Mn^{5+} and helps to oxidize the dye molecule faster [35].

4. Conclusion

Very good morphology Mn_2O_3/TiO_2 nanofibers can be synthesized by calcination of electrospun nanofibers composed of manganese acetate, titanium isopropoxide and poly(vinylpyrrolidone) in air at 650 °C. The final structure of the composite nanofibers is M_2O_3 NPs-doped TiO_2 nanofibers. Incorporation of the Mn_2O_3 strongly enhances formation of the rutile phase, so no anatase phase can be observed in the titania nanofibers matrix. The synthesized nanofibers have a wide range antibacterial activity as they can be exploited to annihilate the colonization of both of Gram-positive and Gram-negative bacteria. Overall, the prepared Mn_2O_3/TiO_2 nanofibers have been demonstrated to be useful and effective in bactericidal applications and present a reasonable alternative for the development of new bactericides. However, the risk aspects for the application on larger scales and in the environment should be strengthened in future study. Also, the studies on the photodegradation of MB dye clearly reveal that the photocatalytic activity of the Mn_2O_3/TiO_2 nanofibers was higher than that of TiO_2 nanofibers.

Acknowledgment

This work was financially supported by the National Plan for Science & Technology (NPST), King Saud University Project no. 11-NAN1460-02. We thank Mr. T.S. Bae and J.C. Lim, KBSI, Jeonju branch, and Mr. Jong-Gyun Kang, Centre for University Research Facility, for taking high-quality FESEM and TEM images, respectively.

References

[1] H. Matsui, N. Bandou, S. Karuppuchamy, M.A. Hassan, M. Yoshihara, Efficient photocatalytic activity of MnO_2-loaded ZrO_2/carbon cluster nanocomposite materials under visible light irradiation, Ceramics International 38 (2012) 1605–1610.

[2] M. Choi, K.H. Shin, J. Jang, Plasmonic photocatalytic system using silver chloride/silver nanostructures under visible light, Journal of Colloid and Interface Science 341 (2010) 83–87.

[3] M.S. Hassan, T. Amna, O.B. Yang, H.C. Kim, M.S. Khil, TiO_2 nanofibers doped with rare earth elements and their photocatalytic activity, Ceramics International 38 (2012) 5925–5930.

[4] G.T. Lim, K.H. Kim, J. Park, S.H. Ohk, J.H. Kim, D.L. Cho, Synthesis of carbon-dopedphotocatalytic TiO_2 nano-powders by AFD process, Journal of Industrial and Engineering Chemistry 16 (2010) 723–727.

[5] A.R. Unnithan, N.A.M. Barakat, R. Nirmala, S.S. Al-Deyab, H.Y. Kim, Novel electrospun nanofiber mats as effective catalysts for water photosplitting, Ceramics International 38 (2012) 5175–5180.

[6] A. Kudo, Y. Miseki, Heterogeneous photocatalyst materials for water splitting, Chemical Society Reviews 38 (2009) 253–278.

[7] D. Chatterjee, Effect of excited state redox properties of dye sensitizers on hydrogen production through photo-splitting of water over TiO_2 photocatalyst, Catalysis Communications 11 (2010) 336–339.

[8] H.R. Pant, C.H. Park, B. Pant, L.D. Tijing, H.Y. Kim, C.S. Kim, Synthesis, characterization, and photocatalytic properties of ZnO nano-flower containing TiO_2 NPs, Ceramics International 38 (2012) 2943–2950.

[9] H. Kong, J. Song, J. Jang, Photocatalytic antibacterial capabilities of TiO_2-biocidal polymer nanocomposites synthesized by a surface-initiated photopolymerization, Environmental Science and Technology 44 (2010) 5672–5676.

[10] Z. Zhang, W. Wang, M. Shang, W. Yin, Photocatalytic degradation of rhodamine B and phenol by solution combustion synthesized $BiVO_4$ photocatalyst, Catalysis Communications 11 (2010) 982–986.

[11] P. Wongwanwattana, P. Krongkitsiri, P. Limsuwan, U. Tipparach, Fabrication and photocatalysis of nanostructured TiO_2 for solar hydrogen production, Ceramics International 38 (2012) S517–S519.

[12] H.Q. Liu, J.X. Yang, J.H. Liang, Y.X. Huang, C.Y. Tang, ZnO nanofiber and nanoparticle synthesized through electrospinning and their photocatalytic activity under visible light, Journal of the American Ceramic Society 91 (2008) 1287–1291.

[13] H.Y. Guan, C.L. Shao, S.B. Wen, B. Chen, J. Gong, X.H. Yang, Preparation and characterization of NiO nanofibres via an electrospinning technique, Inorganic Chemistry Communications 6 (2003) 1302–1303.

[14] Z.F. Zhou, Y. Feng, W.B. Xu, F.M. Ren, H.H. Ma, Preparation and photocatalytic activity of zinc sulfide/polymer nanocomposites, Journal of Applied Polymer Science 113 (2009) 1264–1269.

[15] C.H. Wang, C.L. Shao, L.J. Wang, L. Zhang, X.H. Li, Y.C. Liu, Electrospinning preparation, characterization and photocatalytic properties of Bi_2O_3 nanofibers, Journal of Colloid and Interface Science 333 (2009) 242–248.

[16] T. Amna, M.S. Hassan, N.A.M. Barakat, D.R. Pandeya, S.T. Hong, M.S. Khil, H.Y. Kim, Antibacterial activity and interaction mechanism of electrospun zinc-doped titania nanofibers, Applied Microbiology and Biotechnology 93 (2012) 743–751.

[17] R. Nirmala, H.Y. Kim, R. Navamathavan, C. Yi, J.J. Won, K.S. Jeon, A. Yousef, R. Afeesh, M. El-Newehy, Photocatalytic activities of electrospun tin oxide doped titanium dioxide nanofibers, Ceramics International 38 (2012) 4533–4540.

[18] M.A. Kanjwal, N.A.M. Barakat, F.A. Sheikh, H.Y. Kim, Electronic characterization and photocatalytic properties of TiO_2/CdO electrospun nanofibers, Journal of Materials Science 45 (2010) 1272–1279.

[19] A. Yousef, N.A.M. Barakat, T. Amna, S.S. Al-Deyab, M.S. Hassan, A. Abdel-hay, H.Y. Kim, Inactivation of pathogenic *Klebsiella pneumoniae* by CuO/TiO_2 nanofibers: a multifunctional nanomaterial via one-step electrospinning, Ceramics International 38 (2012) 4525–4532.

[20] A.R. Armstrong, P.G. Bruce, Synthesis of layered $LiMnO_2$ as an electrode for rechargeable lithium batteries, Nature 381 (1996) 499–500.

[21] A.E. Fischer, K.A. Pettigrew, D.R. Rolison, R.M. Stroud, J.W. Long, Incorporation of homogeneous, nanoscale MnO_2 within ultraporous carbon structures via self-limiting electroless deposition: implications for electrochemical capacitors, Nano Letters 7 (2007) 281–286.

[22] Z. Yang, Y. Zhang, W. Zhang, X. Wang, Y. Qian, X. Wen, S. Yang, Nanorods of manganese oxides: synthesis, characterization and catalytic application, Journal of Solid State Chemistry 179 (2006) 679–684.

[23] J. Fei, Y. Cui, X. Yan, W. Qi, Y. Yang, K. Wang, Q. He, J. Li, Controlled preparation of MnO_2 hierarchical hollow nanostructures and their application in water treatment, Advanced Materials 20 (2008) 452–456.

[24] Z.Y. Yuan, Z.L. Zhang, G.H. Du, T.Z. Ren, B.L. Su, A simple method to synthesise single-crystalline manganese oxide nanowires, Chemical Physics Letters 378 (2003) 349–353.

[25] M.S. Hassan, T. Amna, D.R. Pandeya, A.M. Hamza, Y.Y. Bing, H.C. Kim, M.S. Khil, Controlled synthesis of Mn_2O_3 nanowires by hydrothermal method and their bactericidal and cytotoxic impact: a promising future material, Applied Microbiology and Biotechnology 95 (2012) 213–222.

[26] H. Koyanaka, K. Takeuchi, C.K. Loong, Gold recovery from parts-per-trillion-level aqueous solutions by a nanostructured Mn_2O_3 adsorbent, Separation and Purification Technology 43 (2005) 9–15.

[27] Z. Gui, R. Fan, X.H. Chen, Y.C. Wu, A simple direct preparation of nanocrystalline Mn_2O_3 at ambient temperature, Inorganic Chemistry Communications 4 (2001) 294–296.

[28] X. Chen, X. Li, Y. Jiang, C. Shi, X. Li, Rational synthesis of α-MnO_2 and γ-Mn_2O_3 nanowires with the electrochemical characterization of α-MnO_2 nanowires for supercapacitor, Solid State Communications 136 (2005) 94–95.

[29] W. He, Y. Zhang, X. Zhang, H. Wang, H. Yan, Low temperature preparation of nanocrystalline Mn_2O_3 via ethanol-thermal reduction of MnO_2, Journal of Crystal Growth 252 (2003) 285–288.

[30] A. Rkan, U. Bakir, G. Karakas, Photocatalytic microbial inactivation over Pd doped SnO_2 and TiO_2 thin films, Journal of Photochemistry and Photobiology A 184 (2006) 313–321.

[31] W. Zhang, Y. Chen, S. Yu, S. Chen, Y. Yin, Preparation and antibacterial behavior of Fe^{3+}-doped nanostructured TiO_2 thin films, Thin Solid Films 516 (2008) 4690–4694.

[32] O. Akhavan, Lasting antibacterial activities of Ag–TiO_2/Ag/a-TiO_2 nano-composite thin fico photocatalysts under solar light irradiation, Journal of Colloid and Interface Science 336 (2009) 117–124.

[33] J.P. Xu, S.B. Shi, L. Li, J.F. Wang, L.Y. Lv, F.M. Zhang, Y.W. Du, Effect of manganese ions concentration on the anatase–rutile phase transformation of TiO_2 films, Journal of Physics and Chemistry of Solids 70 (2009) 511–515.

[34] P.K. Stoimenov, R.L. Klinger, G.L. Marchin, K.J. Klabunde, Metal oxide nanoparticles as bactericidal agents, Langmuir 18 (2002) 6679–6686.

[35] T.K. Ghorai, S. Pramanik, P. Pramanik, Synthesis and photocatalytic oxidation of different organic dyes by using Mn_2O_3/TiO_2 solid solution and visible light, Applied Surface Science 255 (2009) 9026–9031.